Visualizing Jets in Crossflow with Classic Schlieren

Sreelekshmi Sreekumar[1], Michelle Franzen[2], Louis Vest[2], Marley Albright[2], Justin Urso[3], and Subith S. Vasu[4]

Center for Advanced Turbomachinery and Energy Research (CATER), Department of Mechanical and Aerospace Engineering, University of Central Florida, Orlando, FL, 32816, USA

Flow visualization is essential for studying fluid behavior and optimizing engineering systems. This work uses classic Schlieren imaging to investigate jets in crossflow within a shock tube, capturing density gradients caused by the jet's interaction with a supersonic primary flow. The experimental set-up incorporated minimal additional mirrors to address spatial constraints while mitigating optical aberrations. A shock tube provided controlled high-speed flow, while a regulated injection system ensured consistent jet properties. A synchronized triggering system coordinated jet activation, diaphragm rupture, and imaging. These findings contribute to understanding jets in crossflow, which is relevant to applications such as turbine cooling and pollutant dispersion.

I. Introduction

Flow visualization is an umbrella term used to describe methods that help understand how fluids behave in various conditions and assist with other needs, such as optimizing engineering designs, validating computer simulations and analytical models, and examining air pollution. It was a method that gained popularity in the late 19th and early 20th century with Ludwig Prandtl's boundary layer concept and August Toepler's Schlieren imaging [1].

Today, there are various types of flow visualization techniques. Tracer visualization methods involve using additional materials to enhance the flow, such as oil films, dye, smoke, clay, bubbles, and tufts [2]; some of these also act as reacting agents that change color or opacity to reveal flow structures. Particle-based visualization techniques track certain particles using high-speed cameras or lasers to identify their motion and velocity fields. There are also advanced techniques such as Acoustic Doppler Velocimetry [3], which uses acoustic waves to measure fluid velocities, Magnetic Resonance Imaging [4] to visualize blood flow, and Infrared Thermography [5] to visualize heat patterns. Optical visualizations also detect variations in refractive index due to density gradients, such as Shadowgraph, Schlieren, Background-Oriented Schlieren, and Interferometry. Computational Fluid Dynamics (CFD) offers modern digital flow visualization using numerical analysis and data structures to simulate a flow field [2]. All visualization techniques present advantages and disadvantages, and multiple techniques are often used to help validate one another, though these techniques on their own provide valuable data if done correctly. All visualization methods can generate qualitative data about a flow field, but only a select few can obtain quantitative data.

One important way these techniques have been implemented is by investigating flight conditions in impulse facilities [6] or wind tunnels [7]. Impulse facilities can generate a short period of high-enthalpy test conditions for testing aerodynamic flow, while wind tunnels are used to study how objects move through the air. Using flow visualization in these environments is important to capture transient phenomena, understand shock wave characteristics and behavior, and identify how flow interacts with any test models in real-time in these facilities. A common flow interaction that has been studied in impulse facilities and wind tunnels is jets in crossflow [8, 9], which occurs when a jet is perpendicularly injected into a primary flow stream. This creates complex flow structures that are

[1] Undergraduate Researcher, Mechanical and Aerospace Engineering, University of Central Florida
[2] Graduate Researcher, Mechanical and Aerospace Engineering, University of Central Florida
[3] Research Assistant Professor, Mechanical and Aerospace Engineering, University of Central Florida
[4] Professor, CATER, Mechanical and Aerospace Engineering, University of Central Florida, AIAA Associate Fellow

widely observed in engineering applications, environmental systems, and natural processes. For example, jets in crossflow are used to cool turbine blades, enhance mixing in combustors, enable thrust vectoring, simulate pollutant or wastewater dispersion in atmospheric and water flows, and delay flow separation or control wake dynamics in vehicles. For these reasons, a jet in crossflow was tested inside an impulse facility and visualized using classic Schlieren imaging to understand the fluid dynamics around the jet in a high-energy environment.

II. Methodology

Classic Schlieren is an optical technique that visualizes density gradients in transparent media by using collimated light, a knife-edge cutoff, and a focused imaging system to reveal variations in the refractive index caused by phenomena such as heat, pressure, or flow [10]. These set-ups can vary in aspects such as distance and angles between the instruments, types of mirrors used, and number of mirrors and lenses.

Astigmatism arises when optical components, such as mirrors or lenses, fail to focus light uniformly in orthogonal planes, leading to image distortions [11]. In Z-type Schlieren set-ups, this aberration can significantly degrade image quality. Utilizing multiple mirrors in Schlieren set-ups can introduce alignment complexities and potential coating imperfections, leading to image degradation. In other words, each additional mirror increases the risk of misalignment and optical aberrations. Additionally, due to space constraints in the room with the Schlieren set-up and end section of the shock tube, there was a limited optical path length without the use of mirrors. It was not possible to use only two concave mirrors with enough space left over to direct the light from the concave mirror to the knife edge and camera. At a minimum, two additional silver mirrors were required to direct the light from the shock tube to the rest of the set-up for optimal image clarity and use of available space. For these reasons, it was decided to add only the minimum required mirrors.

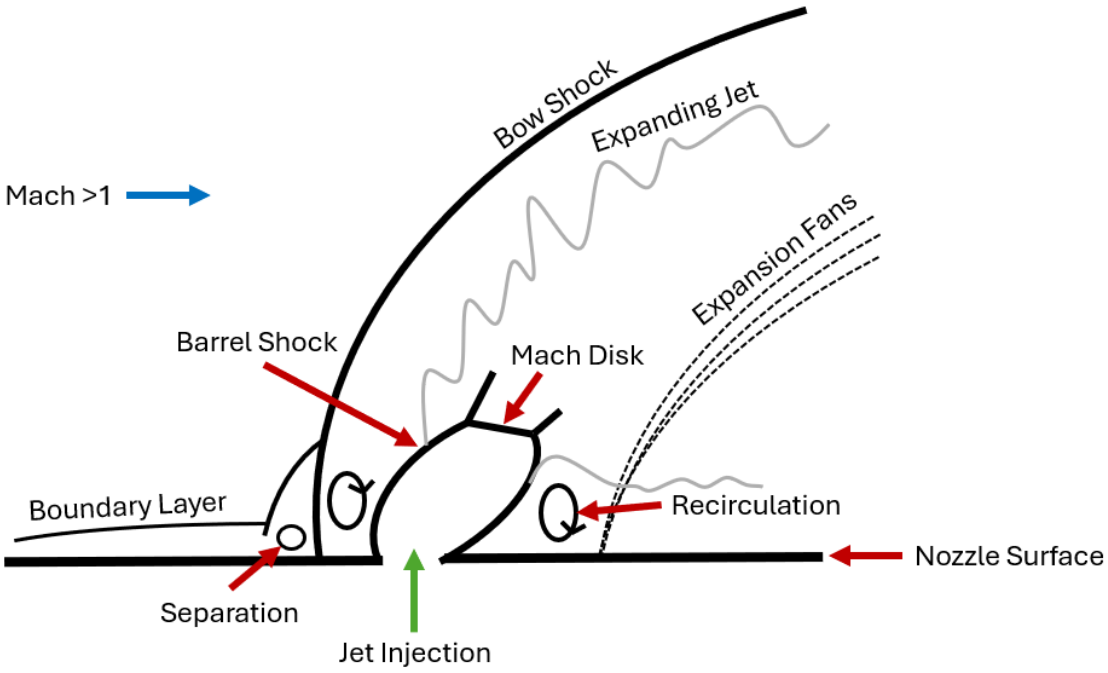

Fig. 1 Close-up of ideal jets in shock tube crossflow structures in Region 2.

The set-up for jets in crossflow involves positioning the injection line near the end of the shock tube, just before the end wall. This placement ensures the jet interacts directly with the developed primary flow within the shock tube as the shock wave passes. The jet is introduced perpendicularly to the crossflow through a simple pipe system, which includes a nozzle to control flow characteristics such as velocity and direction. The properties of the jet, such as velocity, pressure, and composition, are regulated using valves and an actuator, allowing for consistent injection. The primary flow in the shock tube is generated by adjusting the diaphragm pressure ratio, creating either subsonic or supersonic conditions depending on the experimental requirements. The interaction of the jet from the injection line and the shock wave is shown in Fig. 1.

A shock tube is a high-strength experimental device used to study gas dynamics, chemical kinetics, and thermodynamic properties under controlled conditions [12] and creates a high-temperature, high-pressure environment for brief, repeatable experiments. It consists of a high-pressure driver section and a low-pressure driven section separated by a diaphragm, which ruptures to generate an incident shock wave. As this wave propagates at a high velocity (depending on the pressure difference between the driven and driver gas) from the high-pressure section into the low-pressure section, it compresses and heats the gas in its path. Simultaneously, an expansion wave moves in the opposite direction into the high-pressure section. Between the incident shock wave and the expansion wave lies a contact surface, which separates the gas initially in the high-pressure section from the gas in the low-pressure section. The contact surface moves more slowly than the incident shock wave, marking a boundary where the gas velocity changes, but pressure and temperature remain continuous. Once the incident shock reaches the end wall of the shock tube, it bounces off and reflects towards the high-pressure end of the shock tube. Over time, the incident shock wave, reflected shock wave, expansion wave, and contact surface continue to propagate, each influencing the flow and thermodynamic properties of the gas in their respective regions (Fig. 2). For this investigation, the test time is in Region 2 of the shock tube.

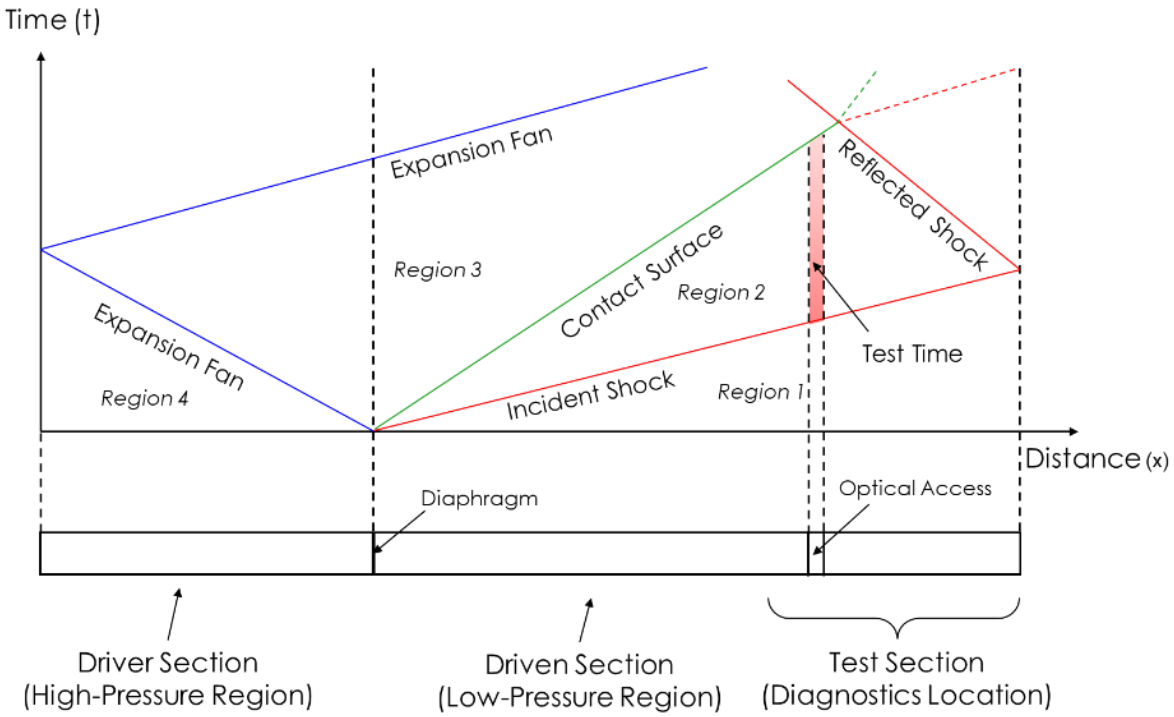

Fig. 2 Shock tube displacement-time diagram.

Shock tubes often include pressure sensors to measure shock velocities and optical ports for non-intrusive diagnostics such as laser absorption spectroscopy and Schlieren imaging. These features enable detailed investigations into phenomena like shock wave propagation, reaction kinetics, and material responses under extreme conditions. Widely used in aerospace, combustion, and material science research, shock tubes provide precise and adaptable tools for understanding high-speed flow and reaction processes.

III. Experimental Set-up

The shock tube experiments were conducted using a high-purity, stainless-steel system designed for precise measurements of gas dynamics and chemical reactions. The shock tube consists of two main sections: the driver and the driven sections, separated by thin Lexan diaphragms, which can vary in thickness. The diaphragm ruptures when the driver section reaches the critical pressure, generating a shock wave that propagates through the driven section. This configuration ensures reliable shock wave initiation for repeatable experimental conditions. The driven section, where the test mixture is introduced, is initially vacuumed to ultra-low pressures (less than 5×10^{-5} torr) using a vacuum pump (Agilent DS102) and, if required, a turbo-molecular pump (Agilent V301). The shock wave's

propagation is tracked using five piezoelectric pressure transducers (PCB Piezotronics 113B26) spaced along the last 1.4 m of the shock tube. These transducers, with a frequency response of 5 kHz, are connected to four time-interval counters (Agilent 53220A). These parameters are also monitored using a high-precision Kistler type 603B1 pressure transducer located 2 cm from the end wall. An NI USB 6009 DAQ was used to keep track of the information coming from the shock tube and diagnostics set-up. More information about this shock tube can be found in Refs. 13 - 20.

The set-up used in this experiment involved mounting two plain silver mirrors, two concave mirrors, a white LED with a 1,000 μm pinhole lens, a razor blade, a 60 mm Nikon lens, and a Photron SA-Z High-Speed Camera on an air table (Fig. 3). This table was located near two sapphire windows near the end wall of the shock tube. The jet flowing perpendicularly to the shock wave was placed between these windows. Light from the LED was aimed at the first concave mirror for collimation, which then passed the light through the sapphire windows onto the silver mirrors. From there, the light was passed onto the second concave mirror to focus the light onto the razor blade. The unblocked light from the razor blade then passes into the camera. The silver mirrors help lengthen the optical path and enhance the sensitivity of refractive index changes, and the razor blade enhances the visibility of the density gradients by creating contrasts in the captured image. Additionally, the pinhole lens focuses the light from the LED while the air table dampens any vibrations that may affect the Schlieren set-up from the shock tube.

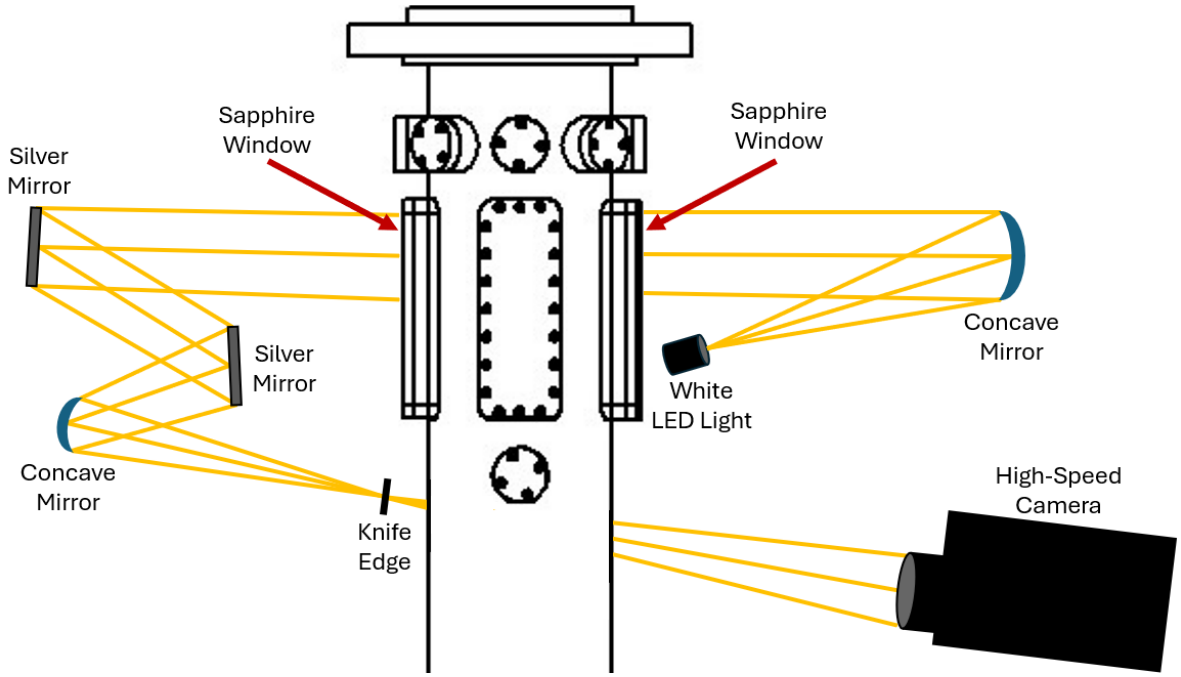

Fig. 3 Top-down view of Schlieren imaging. Black arrows indicate the path of light travel.

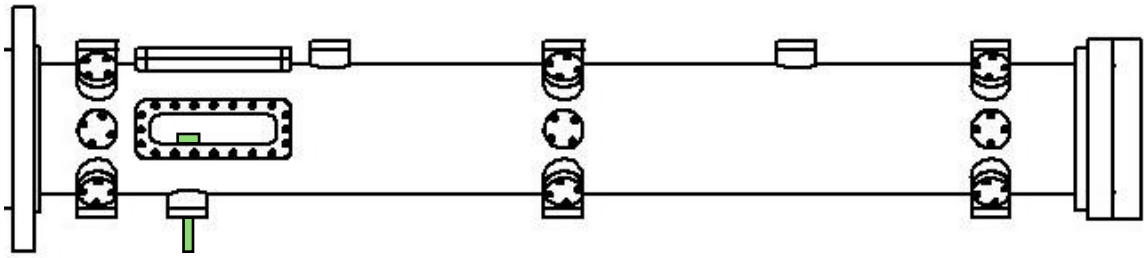

Fig. 4 Side-view schematic of injection line and plug (colored in green) in the test section of the shock tube.

The injection line is placed towards the end of the shock tube right before the end wall. The gas or mixture is injected through a simple pipe system perpendicularly to the shock tube (Fig. 4).

The triggering system in a shock tube experiment ensures precise synchronization of various components, enabling reliable and repeatable data collection. The system coordinates the activation of the jet, actuator, and imaging equipment in a specific sequence to align with the shock wave propagation. The order of operations is critical: the jet is triggered first to allow sufficient time to fully form before interacting with the shock wave. The actuator and camera

are then triggered simultaneously to rupture the diaphragm, generate the shock wave, and ensure imaging captures the interaction correctly. This set-up addresses the limited time between diaphragm rupture and signal activation, ensuring the jet is ready for the test. The actuator trigger introduces a 500 ms delay after the runtime signal to initiate diaphragm rupture, providing precise control over the start of the test. The camera trigger, also delayed by 500 ms, ensures that high-speed imaging captures the fully formed jet interacting with the shock-induced flow. This carefully timed sequence enhances experimental repeatability and ensures accurate jet, shock wave, and diagnostics synchronization.

IV. Results

Theoretically, it is ideal to observe each shock structure of jets in crossflow, as illustrated in Fig. 1. However, due to limitations in the experimental set-up, it is only possible to identify the boundary layer and bow shock in some frames in Fig. 5 - 7. It is difficult to see these structures frame by frame, but they can be identified in videos. During the investigation, it was discovered that the image needs to be as dim as possible using the razor blade to visualize the flow structures better; oversaturation can make certain aspects indistinguishable. Additionally, if any windows are used around the test flow, they must be clean and scratch-free. Some flow structures were blocked by obstructions on the inner side of the sapphire windows. The quality of the diaphragm break affected the number of oblique shocks seen in each shock tube experiment as well as the visibility of certain jet in crossflow structures. The locations of the incident shock on the frames were calculated using a pixel-to-meter conversion provided by the Photron FASTCAM Viewer (PFV4) software. Using this information, it was possible to measure the shock wave velocity within -5% of the calculated FROSH data, which is a Rankine–Hugoniot–equations-based algorithm used to calculate post shock thermodynamic state variables (T2, P2 [21]. For one run, the measured FROSH data stated that the wave velocity was 1781.82 m/s whereas the calculated velocity from the frames was roughly 1736 m/s. The calculated velocity could be slightly lower due to the obstruction or the jet injection nozzle, in the shock tube that is slowing the flow down.

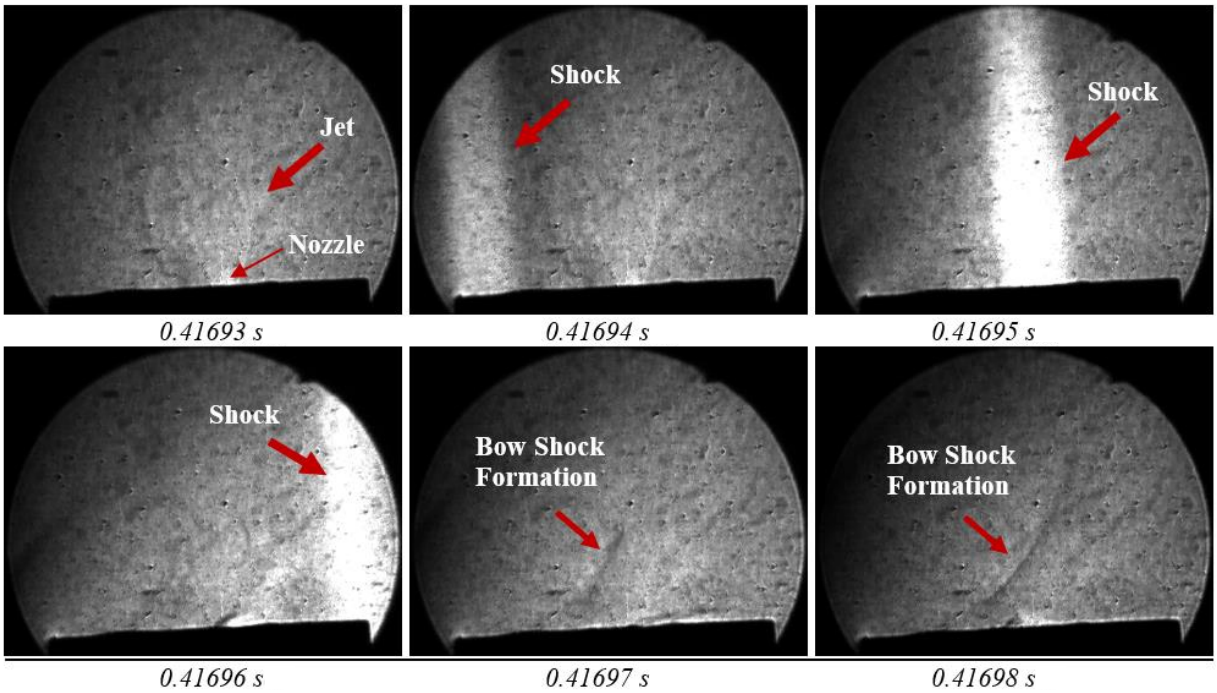

Fig. 5 Incident shock frames.

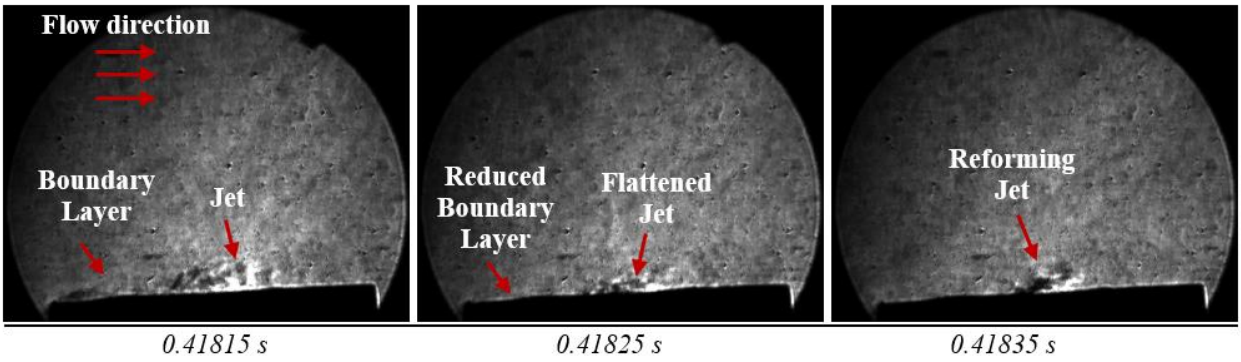

Fig. 6 Contact surface frames.

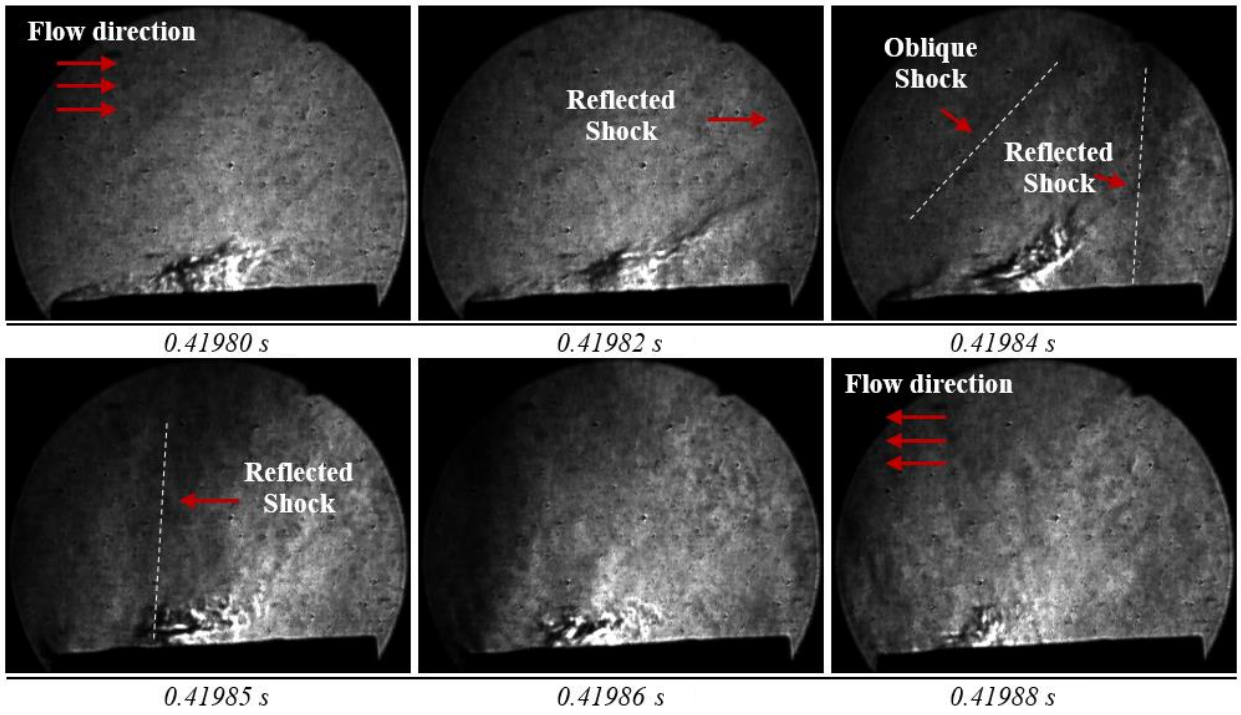

Fig. 7 Reflected shock frames with primary flow directions.

The incident shock wave is shown as a thick, bright vertical line traveling from left to right (Fig. 5). The initial bow shock formation can be seen from 0.41697-0.41698 seconds (Fig. 5). The contact surface follows the incident shock, but it is much more difficult to identify clearly. The indication for the contact surface passing is when the jet is flattened immediately and then emerges shortly after (Fig. 6). The reflected shock can be seen as a black shadow traveling from the right to the left (Fig. 7). Figure 7 also includes some oblique shocks formed due to an imperfect break in the diaphragm.

V. Conclusions

This study successfully employed classic Schlieren imaging to visualize jets in crossflow within a shock tube, capturing critical density gradients resulting from the interaction between the jet and the supersonic primary flow. Despite spatial and optical challenges, the experimental set-up was optimized with minimal additional mirrors, mitigating aberrations while ensuring image clarity. Observations revealed significant flow structures, such as boundary layers, bow shocks, and reflected shocks, although not all structures could be consistently identified frame by frame. The findings demonstrate the applicability of Schlieren imaging in capturing transient flow phenomena in high-energy environments, providing valuable insights into fluid dynamics relevant to turbine cooling, pollutant dispersion, and other engineering applications. Future work could focus on enhancing the resolution of the Schlieren

system and exploring additional techniques to complement the visualization and quantitative analysis of jets in crossflow. Additionally, future work could explore integrating Background-Oriented Schlieren (BOS) techniques into the experimental set-up to complement Schlieren imaging. BOS provides a powerful approach to extracting quantitative data, such as density and temperature distributions, by analyzing displacement fields caused by refractive index gradients through image cross-correlation.

Acknowledgments

The authors thank Daniel Dyson and Dr. Farhan Arafin (both UCF) for their help with experiments. Partial support from UCF and N00178-24-1-0013 (NSWC/JHTO) is acknowledged. The NASA NSTGRO Fellowship (80NSSC23K1185) and the DOD SMART Fellowship support Marley Albright and Louis Vest, respectively.

References

[1] G. S. Settles and M. J. Hargather, "A review of recent developments in schlieren and shadowgraph techniques," *Measurement Science and Technology,* vol. 28, no. 4, p. 042001, 2017.

[2] Yang, W. J., *Handbook of Flow Visualization*, 2nd ed., Routledge, 2001. https://doi.org/10.1201/9780203752876

[3] Kraus, N. C., Lohrmann, A., and Cabrera, R. (1994). "New acoustic meter for measuring 3D laboratory flows." *J. Hydraul. Eng.*, 120(3), 406–412.

[4] Rispoli, V.C., Nielsen, J.F., Nayak, K.S. *et al.* Computational fluid dynamics simulations of blood flow regularized by 3D phase contrast MRI. *BioMed Eng OnLine* 14, 110 (2015). https://doi.org/10.1186/s12938-015-0104-7

[5] Astarita, T., and Carlomagno, G. M., *Infrared Thermography for Thermo-Fluid-Dynamics*, Springer, Berlin, Heidelberg, 2013. https://doi.org/10.1007/978-3-642-21937-8

[6] Störkmann, V., Olivier, H., and Gröning, H., "Force Measurements in Hypersonic Impulse Facilities," AIAA Journal, Vol. 36, No. 3, March 1998, pp. XX–XX. https://doi.org/10.2514/2.402

[7] Baals, D. D., *Wind Tunnels of NASA*, NASA, Washington, DC, 1981.

[8] Getsinger, D. R., Gevorkyan, L., Smith, O. I., and Karagozian, A. R., "Structural and Stability Characteristics of Jets in Crossflow," *Journal of Fluid Mechanics*, Vol. 760, 2014, pp. 342–367. https://doi.org/10.1017/jfm.2014.605

[9] Seiler, F., Gnemmi, P., Ende, H., and others., "Jet Interaction at Supersonic Cross Flow Conditions," *Shock Waves*, Vol. 13, No. 1, 2003, pp. 13–23. https://doi.org/10.1007/s00193-003-0189-y.

[10] Settles, G. S., Schlieren and Shadowgraph Techniques: Visualizing Phenomena in Transparent Media, Springer, Berlin, 2001. https://doi.org/10.1007/978-3-642-56640-0

[11] Prescott, R., and Gayhart, E. L., "A Method of Correction of Astigmatism in Schlieren Systems," *Journal of the Aeronautical Sciences*, Vol. 18, No. 1, 1951, pp. 69. https://doi.org/10.2514/8.1848

[12] Sakthi Balan, G., and Aravind Raj, S., "A Review on Shock Tubes with Multitudinous Applications," *International Journal of Impact Engineering*, Vol. 172, 2023, Article 104406. https://doi.org/10.1016/j.ijimpeng.2022.104406

[13] Higgs, J. P., Pellegrini, J. C., Rahman, R. K., Arafin, F., and Vasu, S. S., "Shock-Tube Measurements of Carbon Monoxide During Combustion of Hydroxyl-Terminated Polybutadiene Products/Air," *AIAA Journal*, Vol. 62, No. 9, Sept. 2024. https://doi.org/10.2514/1.J063500

[14] Rahman, R. K., Wang, C.-H., Masunov, A. E., and Vasu, S., "Experimental and Chemical Kinetic Modeling Study of High-Temperature Oxidation of Diisopropyl Methylphosphonate (DIMP)—A Sarin Simulant," *Combustion and Flame*, Vol. 255, Sept. 2023, Paper 112878. https://doi.org/10.1016/j.combustflame.2023.112878

[15] Rahman, R. K., Barak, S., Wagnon, S. W., Kukkadapu, G., Pitz, W. J., and Vasu, S. S., "Shock Tube Investigation of High-Temperature, Extremely-Rich Oxidation of Several Co-Optima Biofuels for Spark Ignition Engines," *Combustion and Flame*, Vol. 236, Feb. 2022, Paper 111794. https://doi.org/10.1016/j.combustflame.2021.111794

[16] Baker, J. B., Rahman, R. K., Pierro, M., Higgs, J., Urso, J., Kinney, C., and Vasu, S., "Experimental Ignition Delay Time Measurements and Chemical Kinetics Modeling of Hydrogen/Ammonia/Natural Gas Fuels," *Journal of Engineering for Gas Turbines and Power*, Vol. 145, No. 4, 2022, Paper 041002. https://doi.org/10.1115/1.4055721

[17] Ninnemann, E., Pryor, O., Barak, S., Neupane, S., Loparo, Z., Laich, A., and Vasu, S. S., "Reflected Shock-Initiated Ignition Probed via Simultaneous Lateral and Endwall High-Speed Imaging with a Transparent, Cylindrical Test-Section," *Combustion and Flame*, Vol. 224, Feb. 2021, pp. 43–53. https://doi.org/10.1016/j.combustflame.2020.08.017

[18] Johnson, M. S., Nimlos, M. R., Ninnemann, E., Laich, A., Fioroni, G. M., Kang, D., Bu, L., Ranasinghe, D., Khanniche, S., Goldsborough, S. S., et al., "Oxidation and Pyrolysis of Methyl Propyl Ether," *International Journal of Chemical Kinetics*, Vol. 53, No. 8, 2021, pp. 915–938. https://doi.org/10.1002/kin.21489

[19] Rahman, R. K., Barak, S., Manikantachari, K. R. V., Ninnemann, E., Hosangadi, A., Zambon, A., and Vasu, S. S., "Probing the Effects of NOx and SOx Impurities on Oxy-Fuel Combustion in Supercritical CO2: Shock Tube Experiments and Chemical Kinetic Modeling," *Journal of Energy Resources Technology*, Vol. 142, No. 12, 2020, Paper 122302. https://doi.org/10.1115/1.4047314

[20] Laich, A. R., Ninnemann, E., Neupane, S., Rahman, R., Barak, S., Pitz, W. J., Goldsborough, S. S., and Vasu, S. S., "High-

Pressure Shock Tube Study of Ethanol Oxidation: Ignition Delay Time and CO Time History Measurements," *Combustion and Flame*, Vol. 212, Feb. 2020, pp. 486–499. https://doi.org/10.1016/j.combustflame.2019.11.016

[21] Kinney, C., and Vasu, S., "rgfrosh: A Python Package for Calculating Shock Conditions Using Real Gas Equations of State," *Journal of Open Source Software*, Vol. 9, No. 99, 2024, p. 6855. https://doi.org/10.21105/joss.06855